An Open-circuit Fault Diagnosis Method for PMSM Drives Using Symmetrical and DC Components[*]

Wentao Huang[1], Jiachen Du[1], Wei Hua[2] and Qigao Fan[1]*

(1. School of Internet of Things Engineering, Jiangnan University, Wuxi 214122, China;

2. School of Electrical Engineering, Southeast University, Nanjing 201196, China)

Abstract: In this paper, a diagnostic method based on symmetrical and DC components is presented for multiple open-circuit faults (OCFs) in a three-phase permanent magnet synchronous motor drive. The remaining phase currents under faulty situations are theoretically analyzed based on the Fourier series method and the mechanism of torque generation. To evaluate the asymmetry and discriminate fault types, the magnitude ratio of the positive sequence to the negative sequence of phase currents is designed as a fault detection index. Thereafter, the DC components of the phase currents in different reference frames are utilized to locate faults. Specifically, the polarities of the DC contents in the natural reference frame are utilized to locate a single OCF and two OCFs in different legs. Two OCFs in the same leg are diagnosed by evaluating the signs of the phase currents in the *dq* reference frame with a negative rotating direction. The simulated and experimental results validate the effectiveness of the developed method in fault detection and robustness against operating point and motor parameter variations.

Keywords: Permanent magnet synchronous motor, open-circuit fault, fault diagnosis, symmetrical component

1 Introduction

Condition monitoring and fault diagnosis techniques have gained considerable research interest in recent years in the field of electric motor drives[1-3]. The correct fault detection of the machine drive is critical not only as a precondition for fault-tolerant operation but also for scheduling maintenance to improve the reliability and safety of the entire system[4].

The faults in inverters and stators are usually known as electrical faults of machine drives, including short-circuit faults and open-circuit faults (OCFs), which account for the high failure proportion of motor systems[5-6]. Short-circuit faults are typically isolated and converted to OCFs by equipping the motor drive with specific hardware protection circuits because of its severity and destructiveness. Although the OCF may not seriously shut down the drive system, and it can remain undetected for a period, this malfunction may result in overstressing healthy switches, large torque ripples, and mechanical vibration, while even causing secondary failures in other components. Hence, more attention has been paid to the diagnosis of OCF for motor drives.

Existing OCF detection methods can be classified into two main groups: model-based and signal-based methods[7]. Model-based diagnostic techniques are developed by evaluating the consistency between the measured outputs of practical systems and the model-predicted outputs[8-9]. These schemes are load-independent and do not require additional sensors; however, their effectiveness and correctness are highly related to the accuracies of the model and parameter.

Based on the nature of signals, signal-based approaches include the voltage-based method and the current-based method. One of the advantages of the voltage-based technique is its fast detection[10-12]. However, additional voltage sensors or hardware circuits are usually required, which, in many cases is not desirable because it increases the drive cost and

complexity.

A renowned current-based method is Park's vector approach, which has been used successfully for condition monitoring of electric motor drives and diagnosis of several types of malfunctions. It has shown high diagnostic effectiveness and robust performance against false alarms [13-14]. In addition, the motor current signature analysis approach has been widely studied [15-17]. Ref. [15] proposed a three-step method for OCFs in dual three-phase permanent magnet synchronous motor (PMSM) drives. The amplitude and direction of motion of the harmonic currents were used for fault detection. The average absolute values of the phase currents were calculated to locate failures. In Ref. [16], the shape of the current space trajectory associated with different types of OCFs was considered as the fault diagnosis feature. Moreover, a diagnosis method based on current residuals and machine learning models was presented in Ref. [17]. The machine learning algorithm diagnoses faults by comprehensively assessing the current residuals. Recently, model predictive control has been applied in conjunction with current-based diagnostic schemes for condition monitoring and fault detection [18-20]. In Ref. [19], a cost function-based open-phase fault (OPF) diagnostic method was proposed for PMSM drives, where the output of the cost function in the model predictive current control is utilized to monitor the system conditions. The faulty phase was located by the phase angle difference of the currents. Apart from condition monitoring, fault type classification has also been implemented by evaluating the average value of the cost function. The polarities and phase angles of the faulty current vectors were utilized to locate the OCFs in each fault category [20].

The symmetrical component (SC), which contains a large amount of information about the motor voltage or current balance, magnitude, and phase, has been employed as a promising tool in condition analyses [21]. Many proposed approaches that leverage SC characteristics have been presented in the field of fault diagnosis for motor drives [22-24]. With SCs, the phase angle and magnitude of the negative and zero sequence currents were considered as indicators of the stator faults [22]. In Ref. [23], a generalized current SC-based method was proposed for stator and rotor faults of motor drives. Furthermore, the SC theory was extended to a five-phase PMSM drive [24]. The patterns of magnitude and phase angle changes of the fundamental content in the SC were investigated and utilized to identify different types of OPFs. However, considering the OCF diagnosis, most existing SC-based schemes are concentrated on open-phase failures. Studies of multiple OCFs in machine drives are relatively rare.

To diagnose multiple OCFs in PMSM drives, a diagnostic approach based on the SC theory and the current analysis is proposed in this paper. A total of 21 possible combinations of OCFs are investigated in this study. The general characteristics of the phase currents under faulty situations are theoretically analyzed according to the mechanism of torque generation and the SC method. The magnitude ratio of the positive sequence to the negative sequence is calculated and designed as a detection index to discriminate the fault types. Thereafter, the polarities of the phase-current DC components in different reference frames are utilized to locate faulty switches. Consequently, the developed method can correctly diagnose single and multiple OCFs.

The remainder of this paper is organized as follows. In Section 2, the phase currents under four faulty conditions are analyzed based on the Fourier series method and mechanism of torque generation. In Section 3, the principle of the proposed diagnostic method for OCFs is presented. The performance of the proposed scheme is validated by simulations and experiments in Sections 4 and 5, respectively. Finally, the conclusions are presented in Section 6.

2 Current analysis under normal and faulty conditions

2.1 Normal condition

The topology of a two-level voltage-source inverter-fed PMSM drive is illustrated in Fig. 1. Supposing that the stator windings of a PMSM are distributed evenly and symmetrically in space. The phase current and back electromotive force in the three-phase stationary reference frame can be

expressed as

$$\begin{cases} i_a = I_m \sin\theta_e \\ i_b = I_m \sin\left(\theta_e - \dfrac{2\pi}{3}\right) \\ i_c = I_m \sin\left(\theta_e + \dfrac{2\pi}{3}\right) \end{cases} \tag{1}$$

$$\begin{cases} e_a = E_m \sin\theta_e \\ e_b = E_m \sin\left(\theta_e - \dfrac{2\pi}{3}\right) \\ e_c = E_m \sin\left(\theta_e + \dfrac{2\pi}{3}\right) \end{cases} \tag{2}$$

where

$$E_m = -P_r \omega_r \psi_f$$

In addition, I_m is the amplitude of the phase current, θ_e is the electrical angle, and ψ_f is the fundamental magnitude of the phase PM flux linkage. Further, ω_r is the mechanical angular velocity, and P_r is the number of pole pairs.

According to the mechanism of torque generation, the electromagnetic torque equation is derived as

$$\frac{e_a i_a + e_b i_b + e_c i_c}{\omega_r} = T_e \tag{3}$$
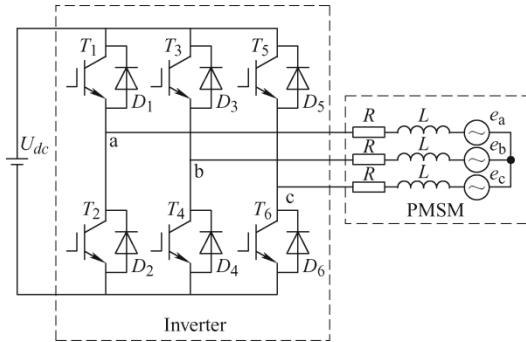

Fig. 1   Schematic of a three-phase PMSM drive

2.2   Faulty condition

Two groups of failures, a single OCF and two OCFs, were investigated in this study. According to the localization and number of faulty devices, a total of 21 OCFs are broadly categorized into four types.

(1) Single OCF.

(2) Two OCFs in two different legs, one in the top switch and the other in the bottom switch.

(3) Two OCFs in two different legs, both of which are in the top or bottom switches.

(4) Two OCFs in the same leg.

If an IGBT is open-circuit, the phase current associated with the faulty leg loses its positive or negative half-cycle. Owing to the star connection, the sum of the three-phase currents is zero, that is, $i_a + i_b + i_c = 0$. After an OCF, the conduction paths of the healthy legs must be changed to maintain current equilibrium.

Assuming that an OCF occurs in IGBT T_1, the current of phase A is limited to flow only in the negative direction. The expression of the faulty phase current can be derived using the Fourier series as follows [25]

$$i_a = I_m \left[\frac{1}{2}\sin\theta_e + \sum_{n=1}^{\infty} \frac{2}{\pi(4n^2 - 1)}\cos(2n\theta_e) + 0.318\,3 \right] \tag{4}$$

where I_m is the amplitude of the phase currents.

For the remaining healthy phases, the instantaneous currents can be deduced using the Lagrange multiplier method [26] as

$$i_j = \frac{T_e^{ref}\sin(\theta_e + \varphi_j)}{\displaystyle\sum_{n=s} P_r \varphi_f \sin^2(\theta_e + \varphi_n)} \tag{5}$$

where T_e^{ref} is the torque reference and $S = \{a, b, c\}$, $j = \{b, c\}$.

Consequently, the expressions of the phase currents for the OCF in IGBT T_1 are summarized as follows

$$\begin{cases} i_a = i_q^{ref}\left[\dfrac{1}{2}\sin\theta_e + \displaystyle\sum_{n=1}^{\infty}\dfrac{2}{\pi(4n^2 - 1)}\cos(2n\theta_e) + 0.318\,3 \right] \\ i_b = i_q^{ref}\sin\left(\theta_e - \dfrac{2}{3}\pi\right) \\ i_c = -i_a - i_b \end{cases} \tag{6}$$

where i_q^{ref} is the q-axis current reference from the output of the speed PI controller.

When two OCFs in the second fault type occur, the phase current related to the faulty switch in the top loses its positive half-cycle, while the other one loses its negative component. Assuming that T_1 and T_4 are open-circuit, the residual currents are expressed as in Eq. (7). Similarly, the expressions of the faulty phase currents associated with the third type can be achieved.

$$\begin{cases} i_a = i_q^{ref}\left[\dfrac{1}{2}\sin\theta_e + \displaystyle\sum_{n=1}^{\infty}\dfrac{2}{\pi(4n^2 - 1)}\cos(2n\theta_e) + 0.318\,3 \right] \\ i_b = i_q^{ref}\left[\dfrac{1}{2}\sin(\theta_e - \dfrac{2}{3}\pi) + 0.318\,3 - \right. \\ \left. \displaystyle\sum_{n=1}^{\infty}\dfrac{2}{\pi(4n^2 - 1)}\cos\left(2n\left(\theta_e - \dfrac{2}{3}\pi\right)\right) \right] \\ i_c = -i_a - i_b \end{cases} \tag{7}$$

When two OCFs simultaneously occur in the same leg, the corresponding phase current becomes null, which is equivalent to an OPF. As a result, the currents in the two other phases are opposite in the phase angle, and their magnitudes increase by a factor of $\sqrt{3}$. For example, when T_1 and T_2 are in the faulty condition, $i_a=i_b+i_c=0$, the following expressions can be deduced

$$\begin{cases} i_a = 0 \\ i_b = \sqrt{3}I_m\left[\sin\left(\theta_e-\dfrac{2}{3}\pi\right)+\dfrac{1}{2}\sin\theta_e\right] \\ i_c = \sqrt{3}I_m\left[\sin\left(\theta_e+\dfrac{2}{3}\pi\right)+\dfrac{1}{2}\sin\theta_e\right] \end{cases} \tag{8}$$

3 Proposed OCF diagnosis method

3.1 Symmetrical component

Based on the SC theory, the phase currents of a three-phase motor drive system can be transformed into three symmetrical components: positive sequence (PS), negative sequence (NS), and zero sequence (ZS) components. As shown in Fig. 1, the motor winding is connected in a star with an isolated neutral point; thus, the ZS content is null. The SC transformation is defined as

$$\boldsymbol{S}=\frac{1}{3}\begin{bmatrix} 1 & 1 & 1 \\ 1 & \beta & \beta^2 \\ 1 & \beta^2 & \beta \end{bmatrix} \tag{9}$$

where $\beta=\exp(j2\pi/3)$.

With the transformation above, the PS and NS components of the phase currents are theoretically obtained as

$$\begin{bmatrix} 0 \\ \overline{I_p} \\ \overline{I_n} \end{bmatrix} = \boldsymbol{S}\begin{bmatrix} \overline{I_a} \\ \overline{I_b} \\ \overline{I_c} \end{bmatrix} \tag{10}$$

where $\overline{I_p}$ and $\overline{I_n}$ are the PS and NS components of the phase A current, respectively.

The sequence components are defined in phasor form as

$$\begin{cases} \overline{I_p} = m_p\angle\varphi_p \\ \overline{I_n} = m_n\angle\varphi_n \end{cases} \tag{11}$$

where m_p/m_n and φ_p/φ_n are the magnitude and phase

angle of the PS and NS components, respectively.

According to the method in Ref. [27], the PS and NS components can be expressed using two rotating reference axes: dq^{+1}, rotating in the positive direction and whose angular position is θ_e, and dq^{-1}, rotating in the negative direction with an angular position of $-\theta_e$. Then, the magnitude and phase angle of the PS components are expressed as

$$\begin{bmatrix} i_{dp} \\ i_{qp} \\ 0 \end{bmatrix} = \boldsymbol{T}\begin{bmatrix} i_a \\ i_b \\ i_c \end{bmatrix} \tag{12}$$

$$\begin{cases} I_{dp} = \dfrac{\omega_e}{2\pi}\displaystyle\int_0^{\frac{2\pi}{\omega_e}} i_{dp}\,\mathrm{d}t \\ I_{qp} = \dfrac{\omega_e}{2\pi}\displaystyle\int_0^{\frac{2\pi}{\omega_e}} i_{qp}\,\mathrm{d}t \end{cases} \tag{13}$$

$$\begin{cases} m_p = \sqrt{I_{dp}{}^2+I_{qp}{}^2} \\ \varphi_p = \arctan\dfrac{I_{dp}}{I_{qp}} \end{cases} \tag{14}$$

where

$$\boldsymbol{T}=\frac{2}{3}\begin{bmatrix} \cos\theta_e & \cos\left(\theta_e-\dfrac{2\pi}{3}\right) & \cos\left(\theta_e+\dfrac{2\pi}{3}\right) \\ -\sin\theta_e & -\sin\left(\theta_e-\dfrac{2\pi}{3}\right) & -\sin\left(\theta_e+\dfrac{2\pi}{3}\right) \\ \dfrac{1}{2} & \dfrac{1}{2} & \dfrac{1}{2} \end{bmatrix}$$

Similarly, the amplitude and phase angle of the NS component are obtained. Substituting Eqs. (4) and (6) into Eq. (13), the dq-axis components in the two rotating references are presented in Eqs. (15) and (16), respectively, as follows

$$\begin{cases} i_{dp} = i_q^{ref}\cos\theta_e(0.141\,5-0.070\,7\cos^2\theta_e+ \\ \quad 0.333\,4\sin\theta_e+0.212\,2\sin^2\theta_e) \\ i_{qp} = i_q^{ref}(0.833\,4+0.166\,7\cos2\theta_e- \\ \quad 0.282\,9\sin\theta_e+0.070\,7\sin3\theta_e) \end{cases} \tag{15}$$

$$\begin{cases} i_{dn} = i_q^{ref}\cos\theta_e(0.141\,5-0.070\,7\cos^2\theta_e- \\ \quad 1.666\,7\sin\theta_e+0.212\,2\sin^2\theta_e) \\ i_{qn} = i_q^{ref}(0.166\,7+0.282\,9\sin\theta_e+ \\ \quad 0.833\,4\cos2\theta_e-0.070\,7\sin3\theta_e) \end{cases} \tag{16}$$

The faulty current magnitude is calculated in terms of the average value of the q-axis current reference over the fundamental period

$$I_{mi} = \frac{\omega_e}{2\pi}\int_0^{\frac{2\pi}{\omega_e}} i_q^{ref}\,\mathrm{d}t \tag{17}$$

where $i=\{1, 2, 3, 4\}$.

With the Fourier series of faulty currents, the analytical results of SC magnitudes under four OCF situations are obtained, as listed in Tab. 1. The magnitudes of both the PS and NS components in each type of fault are fixed to constant values while differing from each other. Moreover, the amplitudes of the two sequences indicate the degree of current asymmetry for different fault types, providing a desirable characteristic for classification.

Tab. 1 Analytical results of SC magnitudes under different faulty conditions

Condition	Faulty switch	Magnitude of PS m_p	Magnitude of NS m_n	$F_d=m_p/m_n$
Normal	None	I_m	0	Inf
1	T_1 T_2 T_3 T_4 T_5 T_6	$0.833\ 4I_{m1}$	$0.166\ 7I_{m1}$	5.002 4
2	$T_1\ T_4$ $T_1\ T_6$ $T_2\ T_3$ $T_2\ T_5$ $T_3\ T_6$ $T_4\ T_5$	$0.75I_{m2}$	$0.144\ 4I_{m2}$	5.193 9
3	$T_1\ T_3$ $T_1\ T_5$ $T_3\ T_5$ $T_2\ T_4$ $T_2\ T_6$ $T_4\ T_6$	$0.583\ 3I_{m3}$	$0.220\ 5I_{m3}$	2.645 4
4	$T_1\ T_2$ $T_3\ T_4$ $T_5\ T_6$	$0.866\ 4I_m$	$0.866\ 4I_m$	1

3.2 Fault diagnosis

3.2.1 Fault type classification

According to the results in Tab. 1, the magnitude ratio of the PS component to the NS component is defined as a fault detection (F_d) index to detect fault types and eliminate the impact of the load torque. By selecting appropriate thresholds, different OCF types can be discriminated.

3.2.2 Fault localization

Once the fault type is determined, it is necessary to locate the faulty switch. The above-mentioned theoretical deductions indicate that the signs of the phase-current DC components vary with the faults in the first three types, which can be extracted as the characteristic of fault localization.

For calculation simplification, the polarities of the phase-current DC components are achieved in terms of average values, as shown in Eqs. (18)-(19). In addition, the normalization method is applied to address the issue associated with the operation condition dependence. Tab. 2 summarizes the DC component signs for the OCFs in the first three conditions.

Tab. 2 Signs of current DC components in the first three fault types

Switch	d_A	d_B	d_C	Fault number
T_1	−1	1	1	1
T_2	1	−1	−1	2
T_3	1	−1	1	3
T_4	−1	1	−1	4
T_5	1	1	−1	5
T_6	−1	−1	1	6
$T_1\ T_4$	−1	1	0	10
$T_1\ T_6$	−1	0	1	11
$T_2\ T_3$	1	−1	0	12
$T_2\ T_5$	1	0	−1	13
$T_3\ T_6$	0	−1	1	14
$T_4\ T_5$	0	1	−1	15
$T_1\ T_3$	−1	−1	1	16
$T_1\ T_5$	−1	1	−1	17
$T_3\ T_5$	1	−1	−1	18
$T_2\ T_4$	1	1	−1	19
$T_2\ T_6$	1	−1	1	20
$T_4\ T_6$	−1	1	1	21

$$I_{n\_dc}=\frac{\omega_e}{2\pi}\int_0^{\frac{2\pi}{\omega_e}}\frac{I_n}{\sqrt{i_{np}^2+i_{qp}^2}}\mathrm{d}t \tag{18}$$

$$d_n=\begin{cases}1 & I_{n\_dc}>H \\ 0 & \left|I_{n\_dc}\right|\leqslant H \\ -1 & I_{n\_dc}<-H\end{cases} \tag{19}$$

where H is the hysteresis width, $n=\{a, b, c\}$.

According to Eq. (10), the two residual currents are opposite-phase signals of the same magnitude. The DC component sign of the remaining currents under

OPF conditions cannot be used to identify fault devices because their values are zero. Nevertheless, considering their specific expressions, the fault features can be easily extracted based on the SC theory. Substituting Eq. (10) into Eqs. (14)-(15), the normalized average values of the phase currents in the two rotating reference axes under different OPF conditions are derived, as listed in Tab. 3.

Tab. 3   Normalized average values of phase current on two rotating references axes under OPF conditions

Switch	I_{dp}	I_{qp}	I_{dn}	I_{qn}
$T_1 T_2$	0	0.866 5	0	0.866 5
$T_3 T_4$	0	0.866 5	0.750 4	−0.433 2
$T_5 T_6$	0	0.866 5	−0.750 4	−0.433 2

The normalized average values of the phase current in the dq^{+1}-axis remain unaffected, while those in the dq^{-1}-axis change significantly. Therefore, the polarities of the phase current in the dq^{-1}-axis are employed to locate the OPFs, as listed in Tab. 4.

Tab. 4   Localization results for OPFs

Switch	d_{dn}	d_{qn}	Fault number
$T_1 T_2$	0	1	7
$T_3 T_4$	1	−1	8
$T_5 T_6$	−1	−1	9

Consequently, a total of 21 OCFs are categorized into four types, which can be identified by the magnitude ratio of the PS to NS components. Then, the specific faults are located by the DC components of the phase currents. A block diagram and a flow diagram of the proposed fault diagnosis method are shown in Fig. 2.
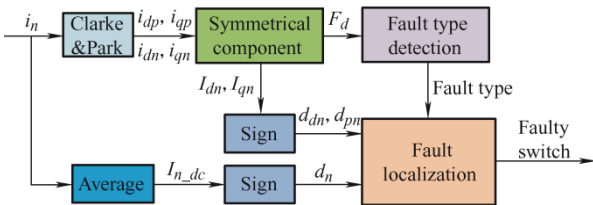

Fig. 2   Block diagram of the proposed fault diagnosis method

4   Simulations

Simulations were conducted in the Matlab/Simulink environment to validate the effectiveness of the developed diagnostic method. The parameters of the three-phase PMSM are listed in Tab. 5. A model predictive current control strategy was employed to regulate the motor drive system. Fig. 3 shows a diagram of the control and diagnosis structures.

Tab. 5   Specifications of the PMSM

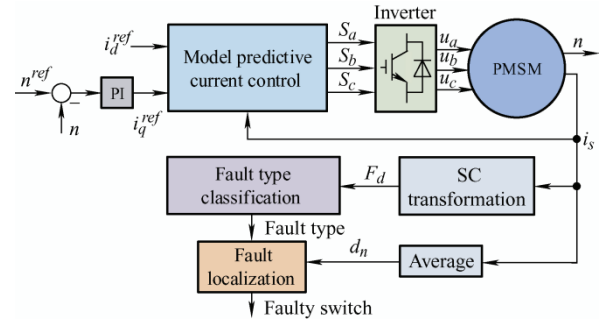| Items	Specifications
Pole pairs of rotor, P_r	4
Phase resistance, R_s /Ω	2.88
d-axis inductance, L_d /mH	6.4
q-axis inductance, L_q /mH	6.4
PM flux-linkage, ψ_f /Wb	0.070 7
Rated speed, n/(r/min)	3 000
Rated torque, T_{en}/(N · m)	2.4
Rated phase current, I_n/A	4

Fig. 3   Diagram of the control and diagnosis structures

The values of the thresholds were first investigated. The reference speed was set to 1 200 r/min with a load of 1.8 N · m. After a large number of tests, the thresholds H and δ_1 are specified as 0.1 A and 7.80, respectively. To avoid an infinite value, the range of the ratio is limited to [0, 12].

The waveforms simulated by the proposed method under the OCF conditions are shown in Fig. 4. When the drive system operates in the normal state, the phase currents are balanced and sinusoidal, and the magnitudes of the PS and NS components of the phase currents are 1 p.u. and zero, respectively. Thus, the fault detection variable is fixed to the upper bound, and the fault number is zero. At the instant t=0.03 s, two OCFs occur simultaneously in T_4 and T_5. The phase currents are no longer balanced, with the positive half-cycle of the phase B current and the negative half-cycle of the phase C current being eliminated. A disturbance can be observed with the amplitude of the PS component, while the NS magnitude increases owing to the asymmetry of the faulty currents. Subsequently, the fault detection index

decreases, and the polarities of the phase current DC components change. Consequently, the fault number stabilizes at 15, suggesting that both T_4 and T_5 are open-circuit. The time of the fault diagnosis is 7.80 ms, which is approximately 62.40% of the motor current cycle (12.50 ms). The simulation results show that the theoretical deduction can provide desirable guidance for faulty current analysis. Meanwhile, the proposed diagnosis method can effectively identify OCFs in a PMSM drive, and the diagnosis time is less than the phase current fundamental period.
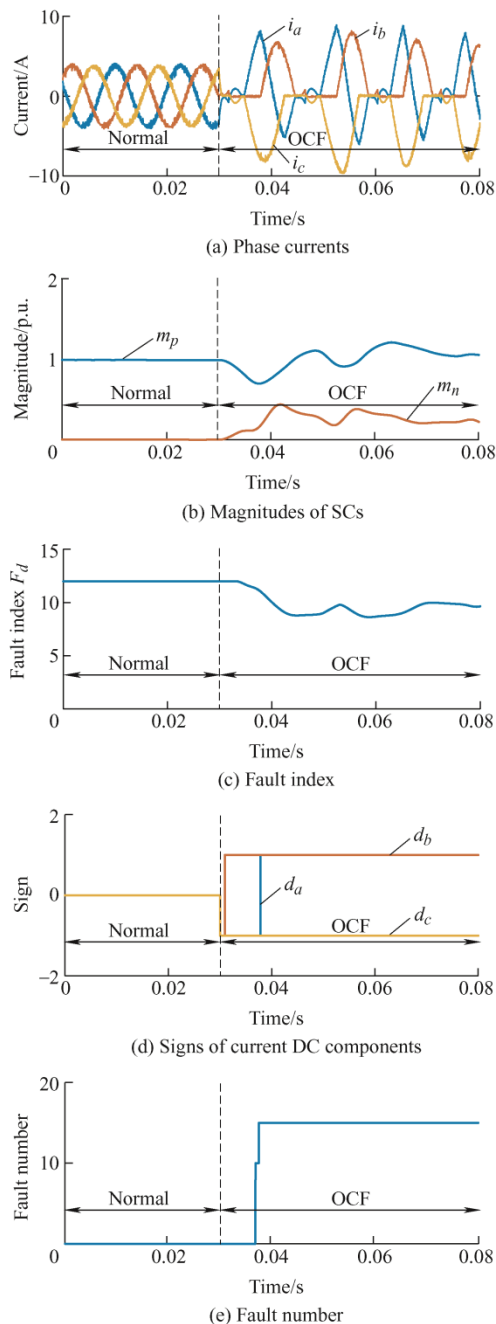
Fig. 4   Simulated waveforms by proposed method under
normal and faulty conditions

5   Experiments

To verify the effectiveness of the proposed control method, experimental validations were conducted on a three-phase PMSM with the same parameters listed in Tab. 5. The test platform setup is shown in Fig. 5. A three-phase PMSM is coupled with a magnetic powder brake, which is used to provide the load torque. A current regulator is employed to adjust the current of the magnetic powder brake. A DC source is adopted to support the DC link voltage, and an Infineon IGBT modular (FP40R12KT3) is used as the inverter. The actual rotor position is obtained using an incremental encoder with 2 500 pulses per revolution. The phase current is measured using a KEN TBC-DS5 current sensor. The control strategy and the proposed fault diagnosis algorithm are implemented in the DSP TMS320F28346 control board, which is embedded in the controller. The sampling frequency is set to 10 kHz. An OCF is implemented by turning off the driving signal of the corresponding switch. Owing to the limitation of channels, only four waveforms, namely the fault detection index, fault number, phase current, and amplitude of the NS component, are captured and presented by an oscilloscope. The values of the four thresholds are obtained after several attempts, as listed in Tab. 6. The upper limit of the fault detection variable is set to 12.
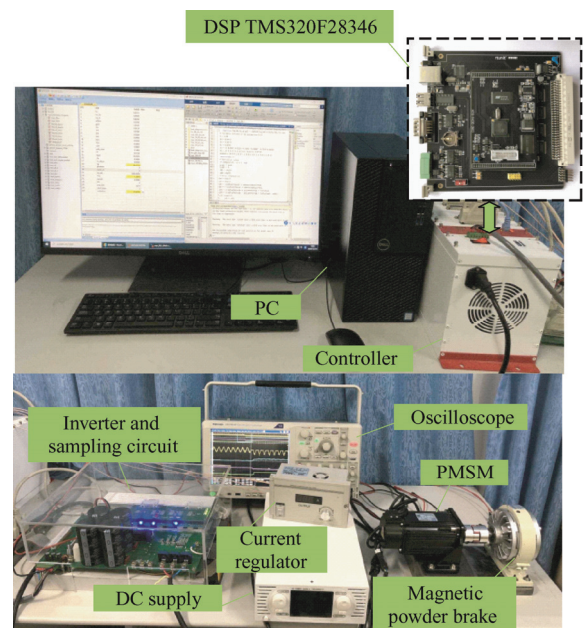

Fig. 5   Experimental platform

Tab. 6   Values of four thresholds

Threshold	H/A	δ_1	δ_2	δ_3	δ_4
Value	0.2	8.00	6.00	3.00	1.20

5.1   OCF test

(1) Single OCF. Fig. 6 shows the experimental waveforms obtained using the proposed diagnostic method for an OCF in IGBT T_1. The PMSM operates at 1 200 r/min with a constant load of 1.8 N • m. Under normal operation, the magnitude of the NS component is nearly null. Thus, the fault detection variable is fixed to the upper limit, and the fault number is zero. When an OCF occurs in T_1, the positive half-cycle of the phase A current is eliminated immediately, and the remaining part is no longer sinusoidal. The amplitude of the NS component increases while the fault detection index decreases and converges to a value near 5.50, which is less than the threshold δ_2. Consequently, the fault number varies from zero to one, which is identical to the theoretical analysis. In the diagnostic process, a transient false number is found with the fault number waveform. This is because the second fault type is identified when the fault index is located in the range of δ_2 to δ_1. The time interval between the failure occurrence and localization is 8.67 ms, which approximately corresponds to 69.36% of the phase current fundamental period.
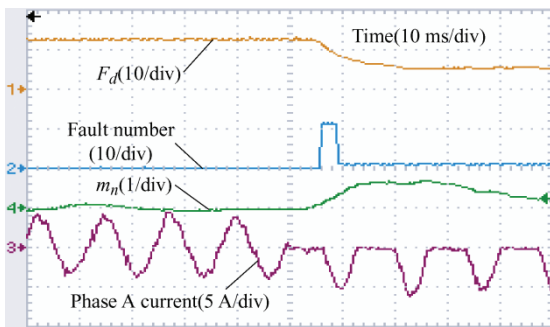

Fig. 6   Experimental results by the proposed method for an OCF in T_1

(2) Two OCFs in the second fault type. The experimental results of the proposed method for the OCFs in T_4 and T_5 are shown in Fig. 7. After the failures, the phase A current becomes nonsinusoidal. Compared with the simulated results in Fig. 4, the amplitude of the experimental phase A current under fault conditions is relatively lower. Meanwhile, the

magnitude of the NS component and the fault detection variable vary in opposition; the former increases and the latter decreases. The index F_d converges to 10, and the fault number steps from 0 to 15, indicating that both T_4 and T_5 are open-circuit. In this state, the switch failure is diagnosed in 8.00 ms, which is approximately 64.00% of the motor current cycle.
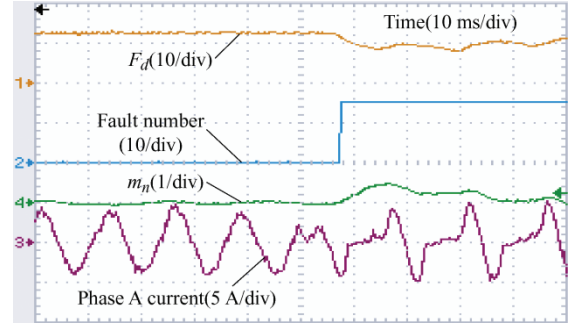

Fig. 7   Experimental results by the proposed method for OCFs in T_4 and T_5

(3) Two OCFs in the third fault type. When two OCFs simultaneously occur in the top switches (T_1 and T_5), the phase A current loses its positive half-cycle, and the magnitude of the remaining component increases, as shown in Fig. 8. In addition, the fault detection variable declines to a value of approximately 2.60, which is located in the range of δ_4 to δ_3. As a result, the fault type is discriminated and the fault number stabilizes at 17, although transient false alarms are generated. The fault is correctly identified with a time interval equivalent to 9.42 ms.
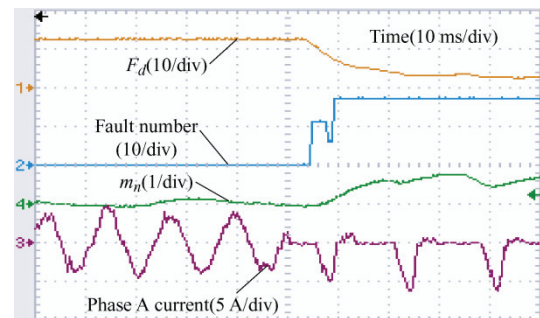

Fig. 8   Experimental results by the proposed method for OCFs in T_1 and T_5

(4) Two OCFs in the same leg. The performance of the proposed method under OPF conditions is shown in Fig. 9. Taking phase A as an example, when both T_1 and T_2 are open-circuit, the phase current becomes null. The amplitude of the NS component is the highest, and the fault detection index is the lowest

among the four faulty conditions. Once the index F_d is less than or equal to δ_4, the OPF is classified. According to the characteristics listed in Tab. 3, the fault number varies from 0 to 7, indicating that the two switches connected to phase A are under faulty scenarios. The time interval between the failure occurrence and localization is 10.20 ms, which corresponds to 81.60% of the phase current fundamental period.
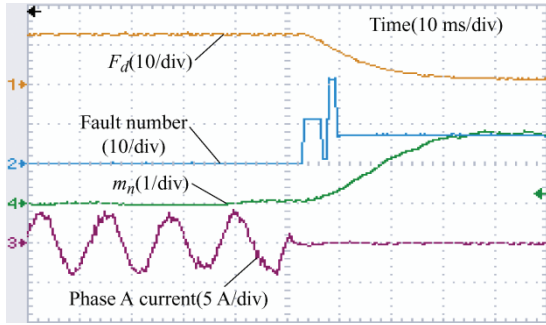

Fig. 9   Experimental results by the proposed method for OCFs in T_1 and T_2

The experimental results verified that the developed approach can detect fault types and locate faulty devices effectively. The diagnosis time for the four types of faults is less than the motor current cycle. In addition, slight discrepancies could be found with the detection time for different fault types owing to the impact of the threshold values.

5.2   Transient performance

To evaluate the robustness of the proposed OCF diagnosis approach, tests with varying loads were performed, as shown in Fig. 10. The speed reference is set to 1 200 r/min. The given load increases from 0.5 N • m to 1.8 N • m, which are corresponding to 20.83% and 75.00% of the rated load, respectively. Because the tension of the magnetic powder brake cannot be adjusted instantaneously, it is difficult to realize an ideal load step in this platform. As shown in Fig. 10, the index F_d remains unchanged in the load variation scenario. Consequently, the fault number remains zero because F_d is fixed to the upper limit. The results indicate that the developed algorithm is load-independent.

A speed variation test was also conducted, as shown in Fig. 11. The reference speed steps from 900 r/min to 1 200 r/min with a constant load of 1.8 N • m. After a temporary adjustment, the phase A current becomes sinusoidal and balanced. In addition, the

amplitude of the NS component recovers to a value near zero after a slight fluctuation, whereas the fault detection index is unchanged. As a result, the fault number remains zero. The experimental results show that the proposed fault diagnosis method is robust to speed variations.
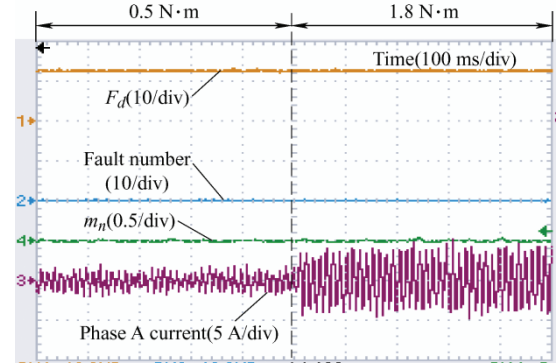

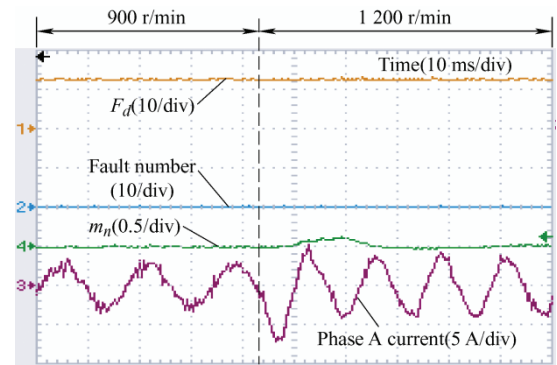Fig. 10   Experimental results under variable speed condition

Fig. 11   Experimental results under variable speed condition

5.3   Comparison analysis

Comparative tests were performed to investigate the superiority of the proposed method. Fig. 12 shows the experimental results of the diagnostic approach in Ref. [20] and the developed method for OCF in T_1 under the parameter mismatch situation. The q-axis inductance is 140% of the nominal value in the predictive current model. In general, the two methods can effectively diagnose OCFs within the phase current fundamental period. Because the cost function is highly associated with the motor parameters, the fault detection index varies under the parameter variation condition. Once this variable is greater than the threshold, a false alarm is generated, as shown in Fig. 12a. In contrast, the developed method is implemented using current components, which are more robust against parameter uncertainties.
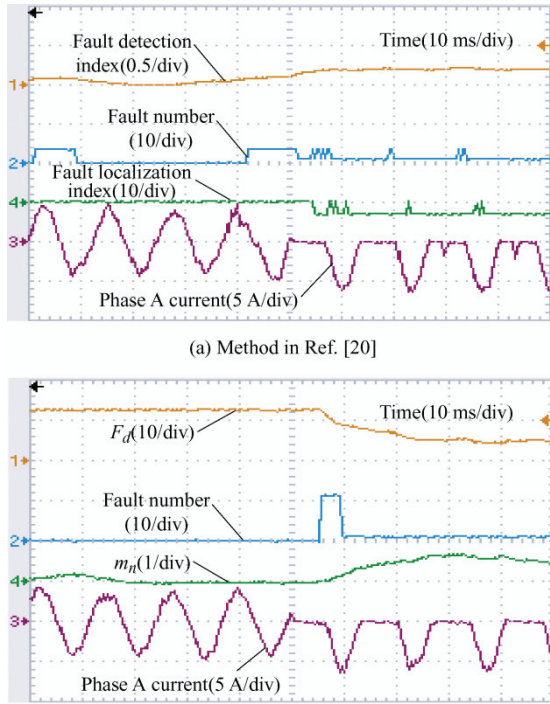
Fig. 12   Experimental results by two diagnostic methods for OCF in T_1 under parameter mismatch condition

Tab. 7 lists the detection time and possible combinations of faulty switches of the proposed algorithm and existing diagnostic approaches. Considering that the developed scheme is related to SCs, average values, and normalized DC currents, the methods in Refs. [13-14, 28] were employed for assessments. The SC-based method in Ref. [24] mainly focuses on OPF detection for a five-phase induction motor drive without considering the diagnosis time. Except for the approach in Ref. [24], the diagnostic time of the other algorithms is less than that of the phase current fundamental cycle. Two Park's vector approach-based methods in Ref. [13] and Ref. [14] can diagnose single and multiple faults. In addition, the normalized DC current method can only identify a single OCF. In contrast, the proposed method can effectively address both single and multiple faults.

Tab. 7   Comparisons among different diagnostic methods

Methods	Fundamental period	Combinations of faulty switches
SC-based [24]	—	15 (OPFs)
Errors of normalized currents Average absolute values [13]	<1	15
Normalized reference current errors [14]	<1	27
Normalized DC current [28]	<1	6
Proposed method	<1	21

6   Conclusions

Based on the SC theory and DC component, a diagnostic approach for OCFs in PMSM drives is presented in this paper. The amplitude ratio of the PS to NS components is employed to monitor the drive conditions and classify the types of failures. The polarities of the phase current DC elements in the natural reference frame are utilized to locate a single OCF and two OCFs in different legs. In addition, the OPF is diagnosed by evaluating the sign of the phase current in the dq^{-1} rotating reference frame. The simulated and experimental results prove that the developed diagnosis algorithm can correctly discriminate and locate a single OCF and two OCFs. The detection time is less than the fundamental phase current period. Moreover, the proposed method shows a desirable robustness against operating point and motor parameter variations.

References

[1] R Wang, J Wang. Fault-tolerant control with active fault diagnosis for four-wheel independently driven electric ground vehicles. *IEEE Trans. Veh. Technol.*, 2011, 60(9): 4276-4287.

[2] W Cao, B C Mecrow, G J Atkinson, et al. Overview of electric motor technologies used for more electric aircraft (MEA). *IEEE Trans. Ind. Electron.*, 2012, 59(9): 3523-3531.

[3] M Riera-Guasp, J A Antonino-Daviu, G Capolino. Advances in electrical machine, power electronic, and drive condition monitoring and fault detection: State of the art. *IEEE Trans. Ind. Electron.*, 2015, 62(3): 1746-1759.

[4] M Cheng, J Hang, J Zhang. Overview of fault diagnosis theory and method for permanent magnet machine. *Chinese Journal of Electrical Engineering*, 2015, 1(1): 21-36.

[5] X Wang, Z Wang, M Gu, et al. Current optimization-based fault-tolerant control of standard three-phase PMSM drives. *IEEE Trans. on Energy Conver.*, 2021, 36(2): 1023-1035.

[6] F Deng, Y Lü, C Liu, et al. Overview on submodule topologies, modeling, modulation, control schemes, fault diagnosis, and tolerant control strategies of modular multilevel converters. *Chinese Journal of Electrical*

Engineering, 2020, 6(1): 1-21.

[7] Z Gao, C Cecati, S X Ding. A survey of fault diagnosis and fault-tolerant techniques—Part I: Fault diagnosis with model-based and signal-based approaches. *IEEE Trans. Ind. Electron.*, 2015, 62(6): 3757-3767.

[8] Q An, L Z Sun, K Zhao, et al. Current residual vector-based open-switch fault diagnosis of inverters in PMSM drive systems. *IEEE Trans. Power Electron.*, 2015, 30(5): 2814-2827.

[9] B Gou, X Ge, S Wang, et al. An open-switch fault diagnosis method for single-phase PWM rectifier using a model-based approach in high-speed railway electrical traction drive system. *IEEE Trans. Power Electron.*, 2016, 31(5): 3816-3826.

[10] J Hang, J Zhang, M Cheng, et al. Detection and discrimination of open-phase fault in permanent magnet synchronous motor drive system. *IEEE Trans. Power Electron.*, 2016, 31(7): 4697-4709.

[11] Q An, L Sun, K Zhao, et al. Switching function model-based fast-diagnostic method of open-switch faults in inverters without sensors. *IEEE Trans. Power Electron.*, 2011, 26(1): 119-126.

[12] K Bi, Q An, J Duan, et al. Fast diagnostic method of open circuit fault for modular multilevel DC/DC converter applied in energy storage system. *IEEE Trans. Power Electron.*, 2017, 32(5): 3292-3296.

[13] J O Estima, A J Marques Cardoso. A new approach for real-time multiple open-circuit fault diagnosis in voltage-source inverters. *IEEE Trans. Ind. Applicat.*, 2011, 47(6): 2487-2494.

[14] J O Estima, A J M Cardoso. A new algorithm for real-time multiple open-circuit fault diagnosis in voltage-fed PWM motor drives by the reference current errors. *IEEE Trans. Ind. Electron.*, 2013, 60(8): 3496-3505.

[15] X Wang, Z Wang, Z Xu, et al. Comprehensive diagnosis and tolerance strategies for electrical faults and sensor faults in dual three-phase PMSM drives. *IEEE Trans. Power Electron.*, 2019, 34(7): 6669-6684.

[16] K Li, S Cheng, T Yu, et al. An on-line multiple open-circuit fault diagnostic technique for railway vehicle air-conditioning inverters. *IEEE Trans. Veh. Technol.*, 2020, 69(7): 7026-7039.

[17] Z Zhang, G Luo, Z Zhang, et al. A hybrid diagnosis method for inverter open-circuit faults in PMSM drives. *CES Transactions on Electrical Machines and Systems*, 2020, 4(3): 180-189.

[18] J Hang, J Zhang, M Xia, et al. Interturn fault diagnosis for model-predictive-controlled-PMSM based on cost function and wavelet transform. *IEEE Trans. Power Electron.*, 2020, 35(6): 6405-6418.

[19] J Hang, H Wu, J Zhang, et al. Cost function-based open-phase fault diagnosis for PMSM drive system with model predictive current control. *IEEE Trans. Power Electron.*, 2021, 36(3): 2574-2583.

[20] W Huang, J Du, W Hua, et al. Current-based open-circuit fault diagnosis for PMSM drives with model predictive control. *IEEE Trans. Power Electron.*, 2021, 36(9): 10695-10704.

[21] A Bellini, F Filippetti, C Tassoni, et al. Advances in diagnostic techniques for induction machines. *IEEE Trans. Ind. Electron.*, 2008, 55(12): 4109-4126.

[22] M B K Bouzid, G Champenois. New expressions of symmetrical components of the induction motor under stator faults. *IEEE Trans. Ind. Electron.*, 2013, 60(9): 4093-4102.

[23] X F St-Onge, J Cameron, S Saleh, et al. A symmetrical component feature extraction method for fault detection in induction machines. *IEEE Trans. Ind. Electron.*, 2019, 66(9): 7281-7289.

[24] A Arafat, S Choi, J Baek. Open-phase fault detection of a five-phase permanent magnet assisted synchronous reluctance motor based on symmetrical components theory. *IEEE Trans. Ind. Electron.*, 2017, 64(8): 6465-6474.

[25] D U Campos-Delgado, J A Pecina-Sanchez, D R Espinoza-Trejo, et al. Diagnosis of open-switch faults in variable speed drives by stator current analysis and pattern recognition. *IET Electr. Power App.*, 2013, 7(6): 509-522.

[26] H Guo, S Guo, J Xu, et al. Power switch open-circuit fault diagnosis of six-phase fault tolerant permanent magnet synchronous motor system under normal and fault-tolerant operation conditions using the average current Park's vector approach. *IEEE Trans. Power Electron.*, 2021, 36(3): 2641-2660.

[27] P Rodriguez, J Pou, J Bergas, et al. Decoupled double synchronous reference frame PLL for power converters control. *IEEE Trans. Power Electron.*, 2007, 22(2): 584-592.

[28] K Rothenhagen, F W Fuchs. Performance of diagnosis methods for IGBT open circuit faults in three phase voltage source inverters for AC variable speed drives.

2005 European Conference on Power Electronics and Applications, Dresden, 2005: P1-P10.

Wentao Huang received the Ph.D. degree in Electrical Engineering from Southeast University, Nanjing, China, in 2020. From January 2018 to January 2019, he was a joint-supervised Ph.D. student with the School of Electrical and Data Engineering, University of Technology Sydney, NSW, Australia.

Since 2020, he has been with Jiangnan University, Wuxi, China, where he is currently a Lecturer with the School of Internet of Things Engineering. His major research interests include permanent magnet machine drives, fault diagnosis and fault-tolerant control.

Jiachen Du received the B.Sc. degree in 2020 from the School of Internet of Things Engineering, Jiangnan University, Wuxi, China, where he is currently working toward the M.Sc. degree in Energy and Power Engineering.

His research interests include permanent magnet synchronous motor drive and fault diagnosis.

Wei Hua (M'03-SM'16) received B.Sc. and Ph.D. degrees both in Electrical Engineering from the School of Electrical Engineering, Southeast University, Nanjing, China, in 2001 and 2007, respectively. During 2004.9-2005.8, he visited the Department of Electronics and Electrical Engineering, The University of Sheffield, UK, as a joint-supervised Ph. D. student.

Since 2007, he has been with Southeast University, where he is currently a Chief Professor with the School of Electrical Engineering. He is the author or co-author of over 140 technical papers, and he is the holder of 60 patents in his areas of interest. His teaching and research interests include the design, analysis, and control of electrical machines.

Qigao Fan received the Ph.D. degree in Mechatronic Engineering from the School of Mechatronic Engineering, China University of Mining Technology, Xuzhou, China, in 2013.

Since 2013, he has been with Jiangnan University, Wuxi, China, where he is currently an Associate Professor with the School of Internet of Things Engineering. From September 2018 to September 2019, he was a Visiting Scholar with the Department of Mechanical and Industrial Engineering, University of Toronto. His teaching and research interests include motor control, robotics, intelligent sensors, and IoT technology.